

**X-ray absorption spectroscopy of biomimetic dye molecules for solar cells**Peter L. Cook,<sup>1</sup> Xiaosong Liu,<sup>1</sup> Wanli Yang,<sup>2</sup> and F. J. Himpsel<sup>1,a)</sup><sup>1</sup>*Department of Physics, University of Wisconsin Madison, 1150 University Ave., Madison, Wisconsin 53706, USA*<sup>2</sup>*Advanced Light Source, Lawrence Berkeley National Laboratory, Berkeley, California 94720, USA*

(Received 15 July 2009; accepted 11 October 2009; published online 16 November 2009)

Dye-sensitized solar cells are potentially inexpensive alternatives to traditional semiconductor solar cells. In order to optimize dyes for solar cells we systematically investigate the electronic structure of a variety of porphyrins and phthalocyanines. As a biological model system we use the heme group in cytochrome c which plays a role in biological charge transfer processes. X-ray absorption spectroscopy of the N 1s and C 1s edges reveals the unoccupied molecular orbitals and the orientation of the molecules in thin films. The transition metal 2p edges reflect the oxidation state of the central metal atom, its spin state, and the ligand field of the surrounding N atoms. The latter allows tuning of the energy position of the lowest unoccupied orbital by several tenths of an eV by tailoring the molecules and their deposition. Fe and Mn containing phthalocyanines oxidize easily from +2 to +3 in air and require vacuum deposition for obtaining a reproducible oxidation state. Chlorinated porphyrins, on the other hand, are reduced from +3 to +2 during vacuum deposition at elevated temperatures. These findings stress the importance of controlled thin film deposition for obtaining photovoltaic devices with an optimum match between the energy levels of the dye and those of the donor and acceptor electrodes, together with a molecular orientation for optimal overlap between the  $\pi$  orbitals in the direction of the carrier transport. © 2009 American Institute of Physics. [doi:10.1063/1.3257621]

**I. MOTIVATION**

The key challenge to photovoltaic power generation is reducing cost. To this end one can pursue two avenues, i.e., increase the efficiency or reduce the cost. Organic molecules in dye-sensitized solar cells<sup>1–12</sup> potentially pursue both avenues by using the tunability and low cost of organic molecules. The idea is to reproduce the light-harvesting and charge transfer properties of biomolecules in simpler organic molecules that contain transition metal centers similar to those in complex metalloproteins. While photosynthesis in plants is not very efficient overall (of the order of 1%), certain reaction steps are very efficient—notably the initial electron-hole separation. The electronic properties of organic molecules are tunable via attaching functional groups. They can be processed roll to roll at low temperatures and the abundance of the raw material should yield low production and material costs.

Metalloproteins involved in electron transport and photosynthesis are characterized by an active center containing a 3d transition metal atom (Mn, Fe) or an alkaline earth (Ca, Mg). The metal is surrounded by a cage of four to six atoms (typically nitrogens). Examples are chlorophyll, hemoglobin, myoglobin, various heme groups, and cytochromes. Photosystem II contains four Mn atoms surrounding a Fe atom. The electrons in the 3d shell of the transition metal are able to change their oxidation state readily and thereby facilitate the separation of electron and hole. Porphyrin derivatives with the 4d transition metal ruthenium have been used

widely for dye-sensitized solar cells. Unfortunately the scarcity of these high Z elements will make scaling up the production of such solar cells prohibitive. Consequently we follow nature and use the 3d transition metals.

The active center of metalloproteins can be reproduced in a variety of small organic molecules, such as porphyrins, phthalocyanines, and their derivatives. In their native state they contain a divalent metal atom surrounded by a planar, fourfold nitrogen cage. The metal atom can be oxidized from the +2 to the +3 oxidation state by electronegative ligands above and below the metal (for example, Cl and CO). Thereby the highest occupied molecular orbital (HOMO) can be shifted between the transition metal and the neighboring nitrogen ligands.<sup>13,14</sup> That provides an opportunity to control the location and separation of electron and hole inside the molecule. Further tailoring of the electronic structure can be achieved by attaching ligands to the outer part of the cloverleaf structure. Particularly important for photovoltaics are the energies of the HOMO and the lowest unoccupied orbital (LUMO). They define the band gap which controls the optical absorption spectrum, and their lineup with the energy levels of the acceptor and donor electrodes controls the separation of electrons and holes. To reduce losses in the charge separation process and thereby increase the open circuit voltage<sup>15</sup> it is desirable to reduce the energy offset of the molecular orbitals in the absorber molecule and the donor/acceptor electrodes while retaining enough of a potential gradient to drive charge separation. An analogous relationship has been found in organic light-emitting diodes (LEDs) be-

<sup>a)</sup>Electronic mail: fhimpsel@wisc.edu.

tween the driving voltage and the position of the HOMO by using various metal phthalocyanines as hole-transporting layer.<sup>16</sup>

The aim of this work is to systematically explore the electronic structure of biomimetic dye molecules by determining their unoccupied orbitals. This is accomplished by near edge x-ray absorption fine structure (NEXAFS) spectroscopy, which measures optical transitions from a specific core level to the lowest unoccupied molecular orbitals including the LUMO. By choosing the metal 2p or the nitrogen 1s core level it is possible to discriminate between orbitals localized at the metal atom and at the surrounding nitrogen cage. From the multiplet structure of the metal 2p edge it is possible to obtain the oxidation state, the spin state, and the ligand field of the metal atom. This can be achieved by comparison to systematic calculations<sup>17–23</sup> or by using reference spectra from model compounds as fingerprints of particular oxidation states and bonding configurations.<sup>22–25</sup> The spin state of the metal atom is also reflected in the multiplet structure. In phthalocyanines a simple relation of the spin state to the branching ratio between the 2p<sub>3/2</sub> and 2p<sub>1/2</sub> absorption edges has been found.<sup>26</sup> Thus, a systematic study of the NEXAFS spectra of biomimetic dye molecules provides a starting point for establishing a database for the associated electronic energy levels and electronic properties. Such a database will be helpful for establishing a tight feedback loop between the design and synthesis of dye molecules and their photovoltaic properties. Ideally, such a program will make it possible to proceed from trial and error to a rational design of tailored molecules for photovoltaics and other optoelectronic applications.

## II. EXPERIMENTAL

### A. Sample preparation

Various types of metal phthalocyanine (M-Pc), and metal octaethyl-porphyrin (M-OEP), as well as equine heart cytochrome *c* were obtained as powders from Sigma-Aldrich. Three types of samples were prepared: (i) powders embedded in carbon tape, (ii) solutions dried on silicon wafers, and (iii) thin films deposited in ultrahigh vacuum onto silicon wafers passivated by their native oxide.

Solutions of Ni-Pc, Cu-Pc, and MnCl-OEP samples were produced mainly using ethanol after testing a few other solvents. Cytochrome *c* samples were made both as powder on carbon tape and also dried water solution. The solutions were dried quickly on a Si(111) with native oxide to minimize the formation of thick crystallites.

Thin films of MnCl-Pc, Fe-Pc, FeCl-Pc, Co-Pc, Mn-OEP, FeCl-OEP, and Co-OEP were produced by sublimation in ultrahigh vacuum from a tantalum Knudsen cell. The substrates were Si(111) wafers covered with the native oxide of about 1 nm thickness. Typical sublimation temperatures for M-Pc were ~430 °C and for M-OEP ~270 °C. The Mn-OEP sample started as MnCl-OEP powder, but was sublimated at 455 °C which is enough to desorb the Cl. The temperature of the Knudsen cell was monitored with a ther-

mocouple with an accuracy of  $\pm 10$  °C. The resulting spectra were independent of the thickness of the film after normalizing the overall intensity.

Film purity was monitored by examining N 1s NEXAFS spectra taken versus evaporation time and temperature. During the initial phase of the evaporation of phthalocyanines, a more volatile impurity was found that exhibited a characteristic  $\pi^*$  transition at 399.5 eV photon energy. It gave way to sublimation of the stable molecule. There was no clear evidence of less volatile residues when the Knudsen cell was heated to higher temperatures after complete evaporation of the molecules. For high purity films a shutter blocked the initial impurity from being deposited.

### B. NEXAFS technique

NEXAFS spectroscopy detects optical transitions from a core level to unoccupied valence orbitals, most notably to the LUMO that corresponds to the acceptor level in an organic solar cell. The binding energy of the core level identifies a specific element and provides clues about its charge state via the chemical core level shift. The core level binding energy can be measured independently by photoelectron spectroscopy. By subtracting the core level binding energy from the NEXAFS transition energy one can obtain an estimate of the energy position of the unoccupied orbital. However, the interaction between the excited valence electron and the core hole shifts the NEXAFS transition energies downward by an unknown amount which depends on the localization of the valence electrons. Nevertheless, a comparison of NEXAFS transition energies for similar transitions in related molecules can be used at the C 1s and N 1s edges to detect systematic trends in the position of the LUMO. For a highly localized transition, such as the transition metal 2p-to-3d edge, a proper calculation of the atomic multiplet structure induced by the electron-hole interaction is required.

The absorption coefficient is measured indirectly by detecting decay products of the core hole, such as Auger electrons and secondary electrons in the total electron yield (TEY) and soft x-ray photons in the fluorescence yield (FY). These signals are proportional to the absorption coefficient as long as the escape depth or the thickness of a thin film sample is small compared to the absorption length of the incoming photons. TEY detection generally operates in this linear regime since the mean free path of electrons (1–10 nm) is small compared to the absorption length of soft x rays (0.1–1  $\mu$ m). FY detection does not always satisfy this criterion since the absorption lengths of incoming and emitted soft x rays are comparable. For quantitative intensity ratios, such as those in Table I, we use TEY detection. FY detection is used to improve the signal/background ratio by filtering out fluorescence from the substrate and selecting the fluorescence from a particular atom.

The most detailed information about the electronic structure (oxidation state, spin state, and crystal field) can be obtained from the transition metal 2p absorption edge, which is dominated by the 2p-to-3d transitions. The 2p level is by far the sharpest core level of the 3d transition metals with an intrinsic Auger lifetime broadening of a few tenths of an eV.

TABLE I. The  $2p_{3/2}/2p_{1/2}$  intensity ratio and peak positions for the 2p-to-3d transitions of phthalocyanines, porphyrins, and cytochrome c. The intensity ratio is determined from the area under the TEY spectra after subtracting the 2p-to-4s continuum (with an accuracy of about  $\pm 0.2$ ).

Molecule	Intensity ratio [ $2p_{3/2}/2p_{1/2}$ ]	$2p_{3/2}$ peak positions (eV)
MnCl-Pc	2.3	639.7, 640.8, 642.2
Mn-OEP <sup>a</sup>	4.2	640.0, 643.4
MnCl-OEP	2.3	639.7, 640.8, 642.0
Fe-Pc	3.1	706.8, 708.5, 709.3
FeCl-Pc	3.2	707.1, 708.8, 709.6
FeCl-OEP	4.0	709.2
Co-Pc	3.4	777.7, 779.7, 781.0
Co-OEP	2.7	777.6, 779.3, 780.6
Ni-Pc	<sup>b</sup>	854.1, 855.5, 856.3
Ni-OEP	2.0	853.6, 855.6
Cu-Pc	<sup>b</sup>	931.6
Cytochrome c	2.0	707.1, 709.3, 712

<sup>a</sup>From MnCl-OEP with the chlorine desorbed in the deposition process.

<sup>b</sup>The intensity ratio is not given because only FY data are available. In that case the intensity ratio is altered by two effects: self-absorption of the  $2p_{1/2}$  fluorescence by the  $2p_{3/2}$  absorption increases the ratio. Saturation of the  $2p_{3/2}$  peak in thick films decreases the value (and dominates in our measurements).

The sensitivity to the 3d states and the narrow width make the 2p edge ideal for extracting the most detailed chemical information about the transition metal center in biomimetic dye molecules.

A full analysis of the fine structure of the transition metal 2p multiplets (such as those in Fig. 1) requires theoretical modeling.<sup>17–23</sup> There are several interactions to be taken into account, such as the screened Coulomb/exchange interaction of the 3d electrons with the 2p core hole and among each other, as well as the ligand field interaction between the 3d electrons and the crystal field induced by the surrounding N atoms. The Coulomb/exchange interaction is sensitive to the oxidation state (here +2 versus +3) and to the spin state. The ligand field interaction is determined by the symmetry group and by parameters for the interaction strength. Phthalocyanines and porphyrins exhibit fourfold planar symmetry ( $D_{4h}$ ), in contrast to cytochrome c where atoms above and below the plane establish a three-dimensional crystal field. A further refinement is the inclusion of configuration interaction,<sup>23</sup> which considers ionic states with charge transfer between the transition metal and its ligands (here N). In the following we will use either published multiplet calculations for our assignments or a simple fingerprinting analysis by comparison with spectra from reference compounds.<sup>22–25</sup> A detailed calculation of the NEXAFS spectra will be pursued separately.

### C. Beamline details and calibration

The measurements were performed at two beamlines at different synchrotron light sources, the VLS PGM at the SRC and Beamline 8.0 at the ALS. A KBr-coated channel plate with an Al filter was used for FY detection. The filter discriminates against the Si substrate emission because the Al 2p edge absorbs the redshifted Si 2p fluorescence.

Radiation damage was avoided by minimizing the exposure to synchrotron light, for example, by working with narrow slits, using variable energy spacing of the data points to focus on the key features, taking a series of spectra to detect changes, closing a shutter between spectra, and spreading the light over an area of  $3 \times 5 \text{ mm}^2$  at the ALS ( $0.1 \times 1 \text{ mm}^2$  at the SRC). The most radiation-sensitive spectral feature was the  $\pi^*$  orbital of the peptide bond in cytochrome c. This and other radiation effects will be reported separately.<sup>27</sup>

All data were calibrated by spectra from reference samples using literature values of peak positions. The calibration was transferred to nearby photon energies by assuming a constant wavelength shift. Carbon 1s spectra were calibrated to the 285.35 eV  $\pi^*$  peak of graphite, nitrogen 1s spectra to the 458.2 eV 2p-to-3d peak of TiO<sub>2</sub> (rutile powder),<sup>28</sup> and metal 2p spectra to the 852.6 eV 2p-to-3d peak of a nickel mesh in the beamline.<sup>29</sup> The Cu 2p FY data were calibrated to the 931.6 eV peak of Cu-Pc.<sup>30</sup> The absolute accuracy of the photon energies is about  $\pm 0.2$  eV, the relative accuracy within a spectrum about  $\pm 0.05$  eV.

The sample current is first divided by the current measured from a Au mesh in the beamline to account for changes in the x-ray flux. The Au mesh is periodically refreshed by *in situ* deposition of new Au onto the mesh. A linear fit based on the pre-edge region is then subtracted from the data to remove the background caused by lower energy transitions. The metal 2p spectra within a given panel are normalized to keep the  $2p_{3/2}$  peak areas constant. The carbon and nitrogen 1s spectra are normalized to have a constant step size from the pre-edge to the continuum level. This corresponds to a normalization per C (or N) atom.

## III. NEXAFS RESULTS

In the molecules discussed here, the HOMO and LUMO are formed either from the nitrogen cage or from the transition metal atom. The close proximity of these orbitals and their significant overlap facilitate electron transfer. This transfer can be controlled by adjusting the orbital energies via ligands.<sup>13,14</sup> In the following, we will first discuss the results concerning thin film oxidation and molecular orientation and proceed to a comparison of the transition metal 2p edges and finally the N and C 1s edges.

### A. Thin film oxidation

Figure 1 demonstrates the effect of sample preparation on the oxidation state of Fe-phthalocyanine. A thin film sample deposited by evaporation in ultrahigh vacuum exhibits a Fe 2p multiplet structure characteristic of Fe<sup>2+</sup> (see Secs. III C 1 and III C 2 for the assignment). This is the native oxidation state of metals in phthalocyanines and porphyrins (without chlorination). The Fe<sup>2+</sup> peak at 706.8 eV gradually disappears after bringing the sample up to air for half a day to a full day (see the two central spectra in Fig. 1). As the Fe<sup>2+</sup> peak disappears a new peak at 709.3 eV appears that is characteristic of Fe<sup>3+</sup>. The bottom spectrum in Fig. 1 is from a dried ethanol solution of as-received Fe-Pc powder and consists almost exclusively of Fe<sup>3+</sup>. Fe-Pc powder embedded

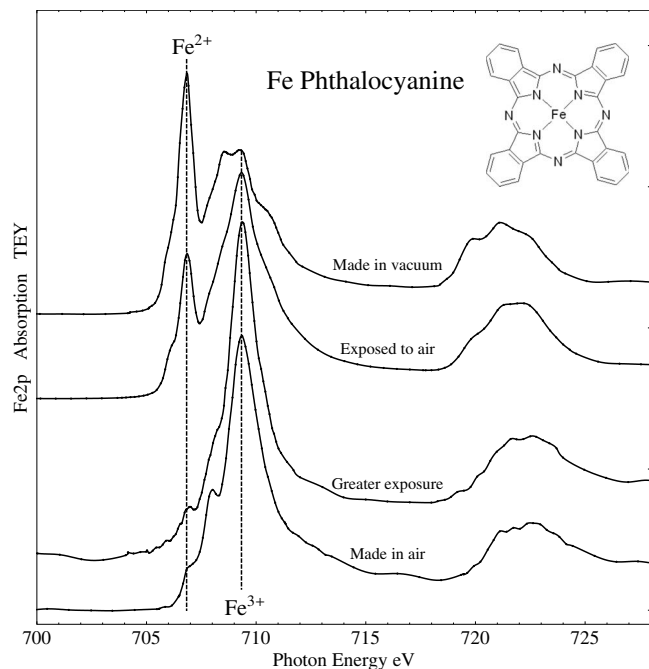


FIG. 1. The Fe 2p absorption edge from differently prepared Fe-phthalocyanine (Fe-Pc) samples. Vacuum deposited Fe-Pc exhibits the native  $\text{Fe}^{2+}$  oxidation state (top). As the sample is exposed to air, the spectrum becomes a mixture of the  $\text{Fe}^{2+}$  and  $\text{Fe}^{3+}$  multiplets (shown for exposures of  $\frac{1}{2}$  and 1 day). A dried ethanol solution of Fe-Pc consists almost completely of  $\text{Fe}^{3+}$  within the probing depth of about 5 nm.

in carbon tape gives a similar spectrum. This indicates that the Fe-Pc is oxidized within the probing depth, which is about 5 nm in the TEY detection mode.

The occurrence of different oxidation states in Fe-Pc depending on the preparation method clearly has consequences on the fabrication of biomimetic solar cells. This situation is reminiscent of the role of water contamination in shortening the lifetime of organic LEDs. It long hampered the production of practical organic LEDs but was eventually solved by proper preparation and sealing methods. Our measurements suggest that biomimetic solar cells could be improved as well by controlling oxidation of thin dye films.

For transition metals with higher atomic number  $Z$  than Fe, we find that phthalocyanines and porphyrins are more stable in the +2 oxidation state while for smaller  $Z$  the +3 oxidation state is favored via oxidation in ambient air. This trend is in line with the decreasing electronegativity of transition metals toward the left of the series.

## B. Molecular orientation

Molecular orientation information in deposited films is obtained from the polarization dependence of the C 1s and N 1s absorption edges (Fig. 2). Optical dipole selection rules for transitions from the 1s core level to the 2p valence orbitals allow transitions for the component of the electric field vector parallel to the orientation of the 2p orbital. As shown in Fig. 2, the transitions into the lowest  $\pi^*$  orbitals are most intense for normal incidence. In that situation the electric field vector lies parallel to the surface and excites  $\pi^*$  orbitals oriented parallel to the surface in the same direction. Since the  $\pi^*$  orbitals are perpendicular to the plane of the mol-

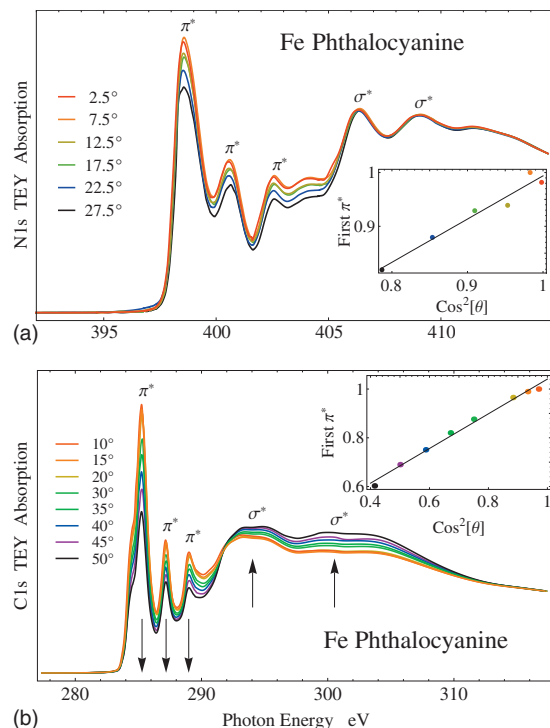


FIG. 2. The polarization dependence of the  $\pi^*$  and  $\sigma^*$  orbitals of a vacuum deposited Fe-Pc film at the N 1s and C 1s absorption edges (top and bottom). The maximum of the  $\pi^*$  intensity at normal incidence ( $\theta=0^\circ$ ) indicates preferential orientation of the molecular plane perpendicular to the surface. The insets show the intensity of the lowest  $\pi^*$  peak as a function of  $\cos^2(\theta)$  using p polarization. The maximum is normalized to 1.

ecule, this observation implies a preferential orientation of the molecular plane perpendicular to the surface, which is typical for the orientation of thick films on oxides<sup>31</sup> and other inert surfaces. Our films are many layers thick. Such perpendicular orientation is also found for other molecules consisting of  $\pi$ -bonded rings. An example is pentacene, where the molecular plane is perpendicular to the surface for thick films, but parallel for a monolayer on a reactive surface.

The molecular orientation can be quantified by modeling. A perfectly parallel orientation of all  $\pi^*$  orbitals would give rise to a  $\cos^2(\alpha)$  intensity distribution, where  $\alpha$  is the angle between the electric field vector and the dynamic dipole of the orbital. Since one measures only one free variable (the polar angle  $\theta$ ), one needs to make specific assumptions about any additional structural parameters to model the system. Here we refrain from making such assumptions and conclude only qualitatively that the slope of the intensity versus  $\cos^2(\theta)$  curves in the inset determines the (model-dependent) order parameter. A slope of 1 would correspond to perfect orientation of the molecular plane perpendicular to the surface, i.e., all  $\pi^*$  orbitals are oriented parallel to the surface. For the lowest  $\pi^*$  orbital we measure slopes of 0.7 (at the C 1s edge) and 0.8 (at the N 1s edge). The polarization dependence of the  $\sigma^*$  orbitals is opposite to that of the  $\pi^*$  orbitals at the C 1s edge, as one would expect from the orthogonal orientation of  $\sigma^*$  versus  $\pi^*$  orbitals. At the N 1s edge this effect is less pronounced. When comparing different molecules and preparation conditions we find substantial variations in the slope of the polarization dependence, i.e.,

the degree of orientation. Clearly there is room for optimizing film quality in the fabrication of dye-sensitized solar cells.

The observed perpendicular orientation of the molecules on SiO<sub>2</sub> is unfavorable for photovoltaic applications where carrier transport takes place perpendicular to the thin film. Orientation parallel to the surface is preferable so that the  $\pi$  orbitals of adjacent molecules overlap optimally. This orientation can be achieved by molecular buffer layers,<sup>31</sup> which suggest an extension of NEXAFS studies to multilayer systems.

### C. Transition metal 2p edges

A systematic series of 2p absorption edges for 3d transition metals was published rather early for phthalocyanines.<sup>32</sup> The transition metal 2p edges varied for different metals while the N 1s edges were rather similar. More recently, it has become possible to resolve considerable fine structure with state-of-the-art photon sources and monochromators, as demonstrated in individual case studies for phthalocyanines and porphyrins.<sup>19,30,33–38</sup> The corresponding core level binding energies<sup>36–41</sup> have been determined in some cases by x-ray photoelectron spectroscopy, and the valence states by soft x-ray emission spectroscopy,<sup>33–37</sup> photoemission,<sup>38,42,43</sup> inverse photoemission,<sup>44</sup> and scanning tunneling spectroscopy.<sup>45,46</sup> Analogous NEXAFS studies exist for porphyrins.<sup>38,47–50</sup>

Here we present a systematic study comparing phthalocyanines and porphyrins—covering a significant part of the 3d metal series. For comparison with biomolecules we add Fe 2p and N 1s spectra for cytochrome c, a metalloprotein that plays a role in reducing photo-oxidized donors in lipid membranes.<sup>12,23</sup> To our knowledge only the much broader Fe 1s edge has been reported for cytochrome c.<sup>51–55</sup>

While fingerprinting methods provide quick information about the oxidation state from the raw data, there is a lot more to be learned from proper theoretical modeling, as discussed in Sec. II B. There are indications that one can also estimate the spin structure from the area ratio of the peaks at the 2p<sub>3/2</sub> and 2p<sub>1/2</sub> edges, using calculation for phthalocyanines as a guide.<sup>26</sup> In that case it was found that the high spin (quintet) configuration has a 2p<sub>3/2</sub>/2p<sub>1/2</sub> ratio larger than the statistical values 2/1, and the intermediate spin (triplet) configuration a smaller ratio. In Fe-porphyrin the intermediate spin (triplet) configuration is the ground state.<sup>56</sup> For possible use in determining the spin configuration we list the experimental peak positions and intensity ratios in Table I. These were obtained from the spectra in Figs. 3–5 by subtracting the 2p-to-4s continuum, which was approximated both by a straight line and by the integral of the spectrum (normalized to the continuum above the 2p edge) with good agreement. It would be interesting to see whether a correlation between the intensity ratio and the spin state can be found for hemelike configurations as well.

#### 1. Cytochrome c Fe 2p edge

Cytochrome c contains a heme core surrounded by a protein shell containing 104 amino acids, as shown in Fig. 3

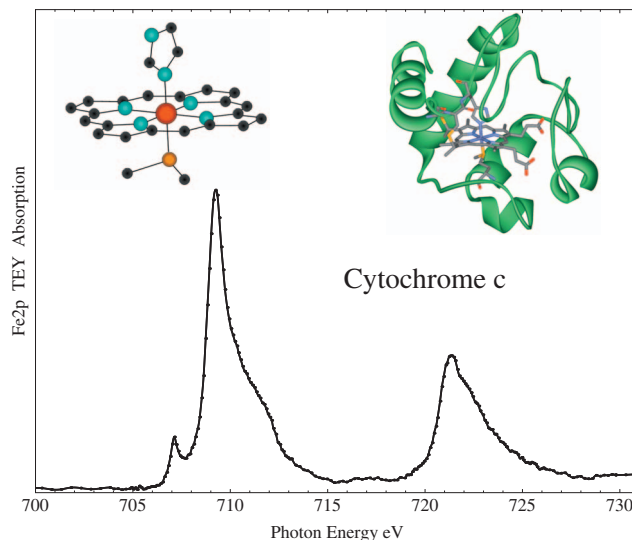


FIG. 3. The Fe 2p NEXAFS spectrum of cytochrome c. The molecular structure consists of a protein skeleton of 104 amino acids surrounding a heme group (see insets; Fe is red, N is blue, S is yellow, and C is black). The signal from the single Fe atom is detected among a background of about a thousand other atoms. The position of the main peak is similar to that in Fe<sup>3+</sup> compounds in Figs. 4 and 5.

(insets). Such heme groups are also found in other biomolecules, such as hemoglobin and myoglobin. These are responsible for charge transfer reactions where the heme cycles between Fe<sup>2+</sup> and Fe<sup>3+</sup>.<sup>23</sup> The heme core resembles the porphyrin structure with a central Fe atom and four surrounding N atoms, but it also exhibits extra out-of-plane ligands, a nitrogen above the Fe, and a sulfur below (blue and yellow at the left inset of Fig. 3). That makes the structure three dimensional and breaks the mirror symmetry about the porphyrin plane.

The Fe 2p spectrum of cytochrome c in Fig. 3 has a dominant peak located at 709.2 eV. The remainder of the 2p<sub>3/2</sub> multiplet consists of a sharp but small peak at 707.1 eV and a broad shoulder at ~712 eV. In the absence of a multiplet calculation including the ligand field appropriate to cytochrome c, one can consider a simple fingerprinting analysis via reference molecules. A comparison between Fe<sup>2+</sup> in ferrocene and Fe<sup>3+</sup> in ferrocenium immobilized at a surface<sup>24</sup> produces reference spectra for different oxidation states of the same molecule. Both oxidation states exhibit doublets consisting of a strong and a weak peak. In Fe<sup>2+</sup> the low energy peak dominates (at 708.5), and in Fe<sup>3+</sup> the high energy peak (at 709.3 eV). This trend is also seen in Fig. 1 when going from vacuum deposited to oxidized Fe-phthalocyanine, i.e., from Fe<sup>2+</sup> to Fe<sup>3+</sup>. Judging from such a qualitative comparison the oxidation state is Fe<sup>3+</sup> in cytochrome c.

A more detailed analysis of the Fe 2p multiplet structure in cytochrome c can be made using a systematic study of molecules containing Fe<sup>3+</sup>, such as Fe(acac)<sub>3</sub>, [FeCl<sub>6</sub>]<sup>3-</sup>,<sup>22</sup> and [Fe<sub>2</sub>(salmp)<sub>2</sub>]<sup>0</sup>.<sup>57</sup> All of these compounds have three-dimensional character with six ligands surrounding the central Fe. This is also true of cytochrome c. Phthalocyanines and porphyrins, on the other hand, have planar, fourfold coordination in the +2 oxidation state and fivefold in the +3 oxidation state.

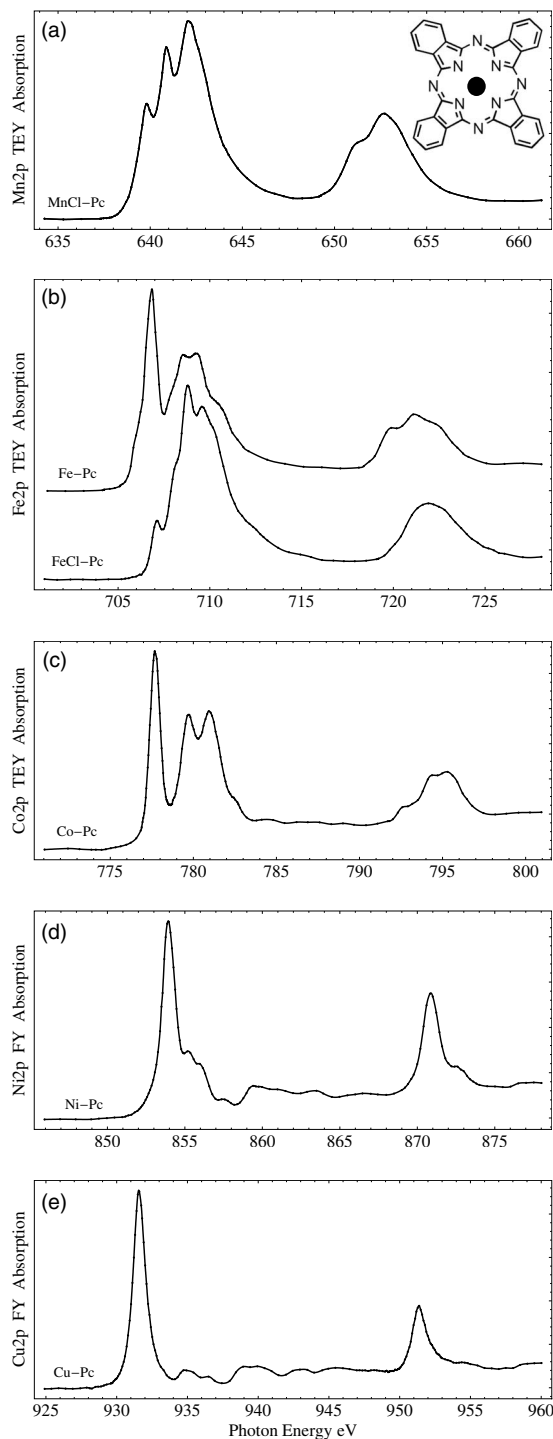


FIG. 4. The transition metal 2p edges from phthalocyanines. The multiplets correspond to the +2 oxidation state for the Pc's and to +3 for chlorinated Pc's.

## 2. Phthalocyanine metal 2p edges

After analyzing the NEXAFS spectrum of a biologically active molecule we proceed to simple organic molecules that mimic the active heme group, specifically phthalocyanines and porphyrins. Figure 4 shows the 2p NEXAFS spectra for a series of phthalocyanines, while Fig. 5 presents similar spectra for porphyrins. Generally, one finds similar dominant peaks in the multiplets for phthalocyanines and porphyrins, as long as the metal atom and its oxidation state are identical.

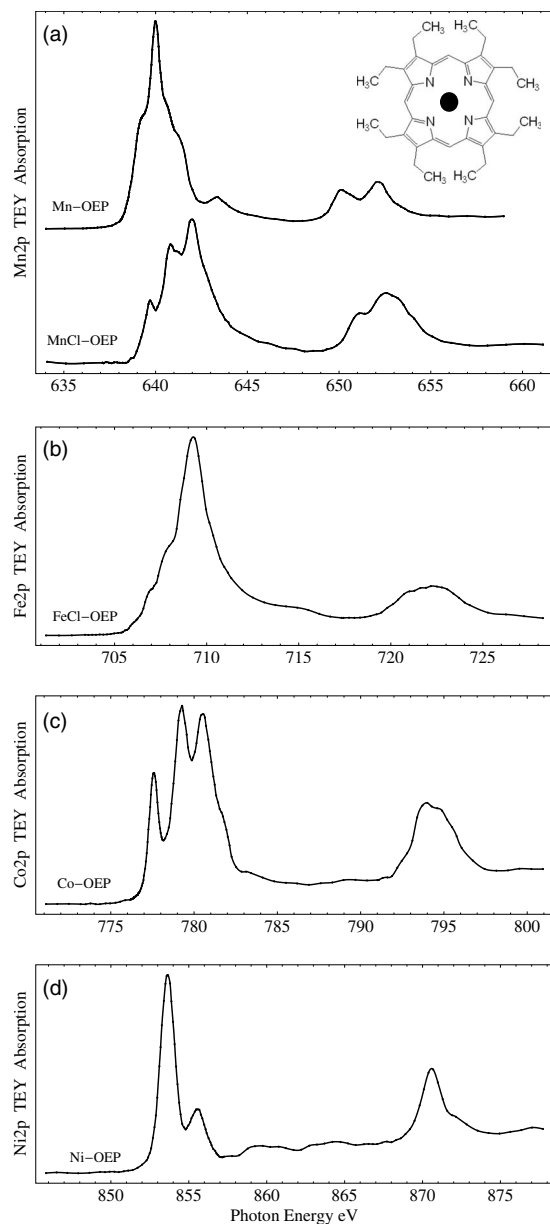


FIG. 5. Similar to Fig. 4 but for porphyrins instead of phthalocyanines. A  $\text{Mn}^{3+}$  multiplet is obtained from an ethanol solution of  $\text{MnCl-OEP}$  at room temperature, while a  $\text{Mn}^{2+}$  multiplet is obtained after desorbing Cl via vacuum deposition of  $\text{MnCl-OEP}$  at the elevated temperature of  $455^\circ\text{C}$ . The multiplet structures of  $\text{Mn}^{2+}$  in  $\text{Mn-OEP}$  and  $\text{Fe}^{3+}$  in  $\text{FeCl-OEP}$  are similar because these are isoelectronic 3d electron configurations.

The latter depends strongly on the sample preparation method, as shown in Sec. III A (Fig. 1). The native oxidation state of the transition metal is +2 in both phthalocyanines and porphyrins, and +3 in their chlorinated modifications.

In the following we discuss the 2p multiplet structures for phthalocyanines containing 3d metals from Mn to Cu. Chlorinated Mn-phthalocyanine ( $\text{MnCl-Pc}$ ) exhibits the characteristic three-peak  $\text{Mn}^{3+}$  multiplet (obtained from calculations of Mn in various oxidation states in Ref. 21). We find a nearly identical multiplet for commercially available  $\text{Mn-Pc}$  itself (not shown), even when evaporated in ultrahigh vacuum. This indicates that  $\text{Mn-Pc}$  is heavily oxidized in air, and that the oxygen is bound so strongly that it does not desorb during evaporation. Comparing this observation with

the behavior of Fe-Pc in Fig. 1 indicates that oxygen seems to be bound more strongly to Mn-Pc than Fe-Pc. That is in line with its lower electronegativity. A  $Mn^{2+}$  multiplet was obtained by evaporating MnCl-OEP at an elevated temperature; see Sec. III C 3.

The multiplet structures of  $Fe^{2+}$  versus  $Fe^{3+}$  have already been introduced with Fig. 1. Essentially, the main  $2p_{3/2}$  peak shifts up by 2.5 eV going from  $Fe^{2+}$  to  $Fe^{3+}$ . Both the native and the chlorinated Fe-Pc are fairly stable. The spectrum of as-received FeCl-Pc powder in Fig. 4 exhibits a remnant of the  $Fe^{2+}$  peak at 706.9 eV (compare Fig. 1). When FeCl-Pc is deposited by vacuum sublimation at 455 °C, this remnant of the  $Fe^{2+}$  peak doubles in height, indicating partial conversion of  $Fe^{3+}$  to  $Fe^{2+}$  by desorption of Cl (not shown).

Going from Fe-Pc to Co-Pc and beyond, the native +2 configuration becomes much more stable against oxidation. The +3 oxidation state cannot be detected anymore, even after long exposure to air. From Co-Pc to Ni-Pc and Cu-Pc the multiplets become narrower and less structured, ending up with a single peak for Cu-Pc. This is due to the decreasing number of 3d holes that couple to the 2p core hole. For  $Cu^{2+}$  there is only one 3d hole left, leading to a single peak (compare Refs. 30 and 33). As the number of 3d holes shrinks, the empty 4s continuum states become visible between the sharp 3d transitions.

### 3. Porphyrin metal 2p edges

Figure 5 shows transition metal 2p NEXAFS spectra of Mn, Fe, Co, and Ni porphyrins, to be compared to those for phthalocyanines in Fig. 4. Generally, one finds rather similar multiplets, but with changes in the intensity ratios and slight variations in the peak positions. This indicates a small but measurable change in the crystal field which can be used to tailor molecules for applications in photovoltaics.

As for Fe-Pc in Fig. 1, different preparation conditions produce different oxidation states for MnCl-OEP (see the top panel of Fig. 5). When thin films of MnCl-OEP are crystallized from ethanol solution on a silicon wafer, the Mn 2p multiplet is characteristic of the +3 oxidation state (compare MnCl-Pc in Fig. 4 and the calculated multiplet structures for Mn in various oxidation states<sup>21</sup>). This oxidation state is expected from the chlorination of MnCl-OEP. However, MnCl-OEP is reduced from +3 to +2 when evaporated in vacuum at a temperature of 455 °C (as opposed to 270 °C for the other OEPs). The oxidation state is again inferred from calculated multiplets in Ref. 21, as well as  $Mn^{2+}$  in Mn-doped ZnS (Ref. 25) (which has the hexagonal wurtzite structure with a locally tetrahedral ligand field). The reduction during high temperature evaporation is likely due to desorption of Cl. This effect needs to be considered in the fabrication of photovoltaic devices. It is interesting to note that the spectrum for reduced MnCl-OEP is very similar to the spectrum of dried photosystem II reported in Ref. 21.

Comparing the  $Mn^{2+}$  and  $Mn^{3+}$  spectra, one finds an upward shift of the dominant peak. That is analogous to the upward shift of the dominant peak when going from  $Fe^{2+}$  to  $Fe^{3+}$  (Figs. 1 and 4). Such an upward shift is not unexpected because the higher oxidation state generates a positive potential that increases the binding energy of the 2p core level.

Although a quantitative explanation is much more involved, it might be worth investigating how far such a crude estimate of the oxidation state can be extended.

Comparing the  $Mn^{2+}$  spectrum with the  $Fe^{3+}$  spectrum provides an opportunity to compare two isoelectronic systems. Coupling the same number of 3d electrons with the  $2p_{3/2}$  core hole produces a similar multiplet structure, consisting of a single peak with weaker features in its tails. This is in contrast to  $Mn^{3+}$  (with one less electron) where one observes three pronounced peaks and to  $Fe^{2+}$  (with an extra electron) where two strong peaks are observed. To pursue this comparison further one might want to consider other isoelectronic combinations, such as  $Fe^{2+}$  and  $Co^{3+}$  or  $Cr^{2+}$  and  $Mn^{3+}$ . However, it is difficult to produce  $Co^{3+}$  and  $Cr^{2+}$  phthalocyanines/porphyrins since these oxidation states are less stable. The Mn and Fe compounds are at the crossover between the +2 and +3 oxidation states. That may also shed light on the special role that they play for charge transfer in metalloproteins.

When comparing transition metal spectra for the same oxidation state, but different surroundings, we observe more subtle changes in the peak intensities, energies, and splittings. Examples are Co-Pc versus Co-OEP and Ni-Pc versus Ni-OEP. These are attributed to changes in the strength of the ligand field. An even larger change is observed when adding extra ligands above and below the four in-plane N atoms when going to cytochrome c (compare FeCl-Pc and FeCl-OEP versus cytochrome c, all in the +3 oxidation state). In that case not only the strength of the ligand field changes but also the symmetry group (from planar to three dimensional).

### D. Nitrogen and carbon 1s edges

The nitrogen 1s edge provides information about the nitrogen cage surrounding the transition metal. Their  $\pi$  and  $\pi^*$  orbitals compete with the 3d electron levels for the HOMO and LUMO, depending on the oxidation state.<sup>16</sup> While the fine structure of the transition metal 2p edge is strongly influenced by the atomic multiplet splitting between the 3d electrons and the 2p core hole,<sup>17,22,23</sup> the N 1s edge better represents the density of states of the unoccupied orbitals (compare the density functional calculations of Alq<sub>3</sub> NEXAFS spectra<sup>58</sup>). The absolute optical transition energy of the observed LUMO is still shifted down by the electrostatic interaction with the N 1s core hole, but one can assume that this electron-hole interaction does not depend strongly on the neighboring transition metal.

Characteristic N 1s NEXAFS spectra are shown in Fig. 6 for phthalocyanines, porphyrins, and cytochrome c (compare also the polarization-dependent N 1s spectra in Fig. 2, top panel). For the phthalocyanines and porphyrins, the shape of the N 1s spectra does not depend much on the transition metal atom (even with chlorination). Only the transition energies are shifted slightly, requiring careful photon energy calibration for meaningful comparisons.

The N 1s spectra of the porphyrins are simpler than those of the phthalocyanines, exhibiting fewer peaks. That can be understood qualitatively from the fact that there is only a single cage of four equivalent N atoms in porphyrins while

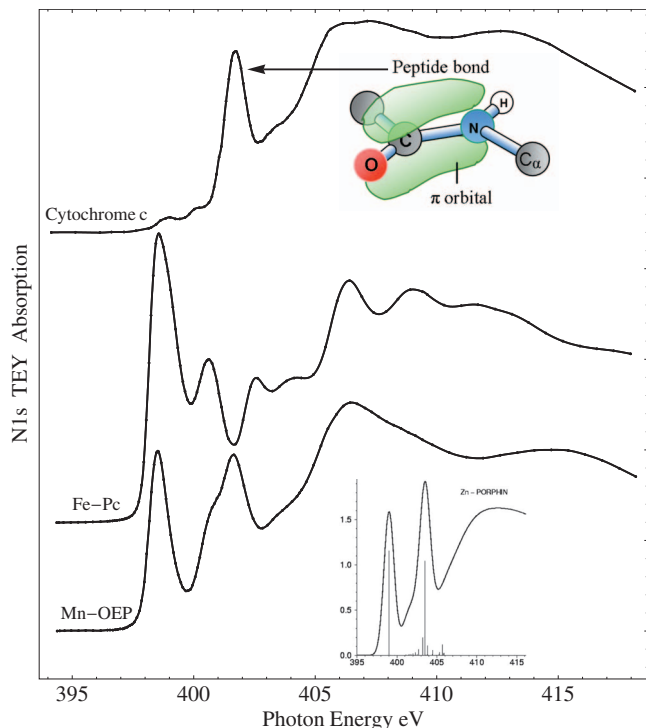


FIG. 6. Comparison of N 1s absorption spectra from an octathyl-porphyrin, a phthalocyanine, and cytochrome c. The Mn-OEP and Fe-Pc spectra are dominated by the transition to the lowest  $\pi^*$  orbital of the N-containing aromatic rings, while the spectrum of cytochrome c is dominated by the higher-lying  $\pi^*$  orbital of the peptide bond. It occurs at 103 locations in the protein backbone and is not directly involved in photosynthesis. The porphyrin data are well described by the calculation for Zn-porphyrin in Ref. 49 (inset). Varying the transition metal and/or the sample preparation conditions causes shifts of a few tenths of an eV in the LUMO of porphyrins, making it possible to tailor the energy levels in dye-sensitized solar cells.

phthalocyanines have two such cages. The calculation in Ref. 49 describes the N 1s spectrum of porphyrins quite well, as shown in the inset of Fig. 6. It uses the static exchange approximation which involves a combination of calculations for the ground state and the excited state. The core hole is taken into account by the  $\Delta$ SCF procedure. Other calculations have determined the charge densities of the lowest  $\pi^*$  orbitals in porphyrins and phthalocyanines and, in particular, their distribution over the transition metal atom and the surrounding nitrogen cage.<sup>59–63</sup>

Generally, the position of the N 1s-to- $\pi^*$  transitions is determined by both the N 1s core level binding energy and the energy position of the unoccupied  $\pi^*$  level. An additional downward shift by electron-hole interaction can be assumed to be the same for different porphyrins. Experimentally we find that the three lowest  $\pi^*$  peaks are almost identical for all Pc's (398.6, 400.6, and 402.6 eV). For OEPs the two dominant  $\pi^*$  peaks vary by up to 0.5 eV (located at 398.5 and 401.6 eV for Mn-OEP). In the OEPs there appears to be a trend toward higher energy with increasing atomic number of the metal. This energy variation is comparable to the variations observed in Ref. 64 for a different type of porphyrin. The preparation method can also shift the transition by such an amount, e.g., varying the evaporation temperatures. The most likely origin of the shift is a change in the position of the  $\pi^*$  orbital because it is delocalized and thus sensitive to

the rearrangement of neighbor molecules. This suggests that the position of the LUMO can be tailored by a several tenths of an eV for optimizing the level alignment in solar cells.

The biological analog cytochrome c displays a completely different N 1s spectrum (Fig. 6 top). It is dominated by a peak at 401.7 eV which corresponds to the  $\pi^*$  orbitals of the 103 peptide bonds between the 104 amino acids. This assignment is based on NEXAFS spectra of other proteins.<sup>65,66</sup> The lower-lying  $\pi^*$  orbitals of the N atoms in the heme group nearly swamped by the large number of peptide bond orbitals.

The C 1s spectra mostly provide information about the orientation of the molecules in thin films (see Fig. 2 bottom and Sec. III B). For the electronic structure the carbon edge is less informative than the transition metal and nitrogen edges because of the large number of inequivalent carbon atoms. They are difficult to discern spectroscopically. If the complex manifold of  $\pi^*$  and  $\sigma^*$  orbitals can be unraveled, the carbon edge might provide helpful information for tailoring the  $\pi$ -to- $\pi^*$  valence transitions. These dominate the strong absorption of the dye molecules in the visible which is important for covering the solar spectrum. It would be interesting to systematically explore changes in the C 1s and N 1s spectra upon attaching functional groups to the molecules. Such changes would provide feedback for tailoring the electronic properties, particularly the creation of electron-hole pairs and their transport to an electrode.

#### IV. CONCLUSIONS AND OUTLOOK

As first step in the biomimetic optimization of molecules for dye-sensitized photovoltaic cells we have performed a systematic spectroscopic study of metallo-organic molecules (phthalocyanines and porphyrins) together with cytochrome c, a biological reference molecule involved in charge transfer. NEXAFS spectroscopy at the transition metal 2p edge reveals the oxidation state, while the nitrogen 1s edge provides the element-resolved density of unoccupied states, including the LUMO. The polarization dependence of the C 1s and N 1s edges yields the orientation of the  $\pi^*$  orbitals which is important for charge transport perpendicular versus parallel to the surface. Controlled preparation of thin film samples is crucial for obtaining the correct oxidation state of the metal atom which is essential for reproducible solar cells. Both oxidation of  $\text{Fe}^{2+}$  to  $\text{Fe}^{3+}$  in air and reduction in  $\text{Mn}^{3+}$  to  $\text{Mn}^{2+}$  during evaporation need to be taken into account. The energy position of the LUMO can be varied by several tenths of an eV via changing the transition metal atom, its oxidation state, and tailoring the surrounding nitrogen cage. Variations in the transition metal multiplet structure between phthalocyanines and porphyrins indicate a change in the ligand field that can be used for tailoring the electronic states. In the future, atomic multiplet calculations would be desirable to quantify the ligand field and the spin state of the transition metal. Density functional calculations would be helpful for revealing the orbital character of the N-derived unoccupied states and for designing new molecules with desirable electronic properties for photovoltaics.

## ACKNOWLEDGMENTS

X.L. acknowledges support by a pre-doctoral fellowship at the ALS. This work was supported by the NSF under Award Nos. DMR-0520527 (MRSEC) and DMR-0084402 (SRC) and by the DOE under Contract Nos. DE-FG02-01ER45917 and DE-AC03-76SF00098 (ALS).

- <sup>1</sup>G. W. Crabtree and N. S. Lewis, *Phys. Today* **60**(3), 37 (2007).
- <sup>2</sup>P. Wang, S. M. Zakeeruddin, J. E. Moser, M. K. Nazeeruddin, T. Sekiguchi, and M. Grätzel, *Nature Mater.* **2**, 402 (2003).
- <sup>3</sup>Y. Bai, Y. Cao, J. Zhang, M. Wang, R. Li, P. Wang, S. M. Zakeeruddin, and M. Grätzel, *Nature Mater.* **7**, 626 (2008).
- <sup>4</sup>M. K. Nazeeruddin, R. Humphry-Baker, D. L. Officer, W. M. Campbell, A. K. Burrell, and M. Grätzel, *Langmuir* **20**, 6514 (2004).
- <sup>5</sup>D. Shi, N. Postrakulchote, R. Li, J. Guo, Y. Wang, S. Zakeeruddin, M. Grätzel, and P. Wang, *J. Phys. Chem. C* **112**, 17046 (2008).
- <sup>6</sup>M. Paulose, K. Shankar, O. K. Varghese, G. K. Mor, and C. A. Grimes, *J. Phys. D: Appl. Phys.* **39**, 2498 (2006).
- <sup>7</sup>W. M. Campbell, A. K. Burrell, D. L. Officer, and K. W. Jolley, *Coord. Chem. Rev.* **248**, 1363 (2004).
- <sup>8</sup>S. Meng, J. Ren, and E. Kaxiras, *Nano Lett.* **8**, 3266 (2008).
- <sup>9</sup>S.-C. Li, J.-G. Wang, P. Jacobson, X.-Q. Gong, A. Selloni, and U. Diebold, *J. Am. Chem. Soc.* **131**, 980 (2009).
- <sup>10</sup>E. I. Solomon, X. Xie, and A. Dey, *Chem. Soc. Rev.* **37**, 623 (2008).
- <sup>11</sup>M. Mohseni, P. Rebertrost, S. Lloyd, and A. Aspuru-Guzik, *J. Chem. Phys.* **129**, 174106 (2008).
- <sup>12</sup>J. Salafsky, J. T. Groves, and S. G. Boxer, *Biochemistry* **35**, 14773 (1996).
- <sup>13</sup>M.-S. Liao and S. Scheiner, *J. Chem. Phys.* **114**, 9780 (2001).
- <sup>14</sup>M.-S. Liao and S. Scheiner, *J. Chem. Phys.* **116**, 3635 (2002).
- <sup>15</sup>R. B. Ross, C. M. Cardona, D. M. Guldi, S. G. Sankaranarayanan, M. O. Reese, N. Kopidakis, J. Peet, B. Walker, G. C. Bazan, E. Van Keuren, B. C. Holloway, and M. Drees, *Nature Mater.* **8**, 208 (2009).
- <sup>16</sup>L. Zhu, H. Tang, Y. Harima, Y. Kunugi, K. Yamashita, J. Ohshita, and A. Kunai, *Thin Solid Films* **396**, 214 (2001).
- <sup>17</sup>F. M. F. de Groot, *J. Electron Spectrosc. Relat. Phenom.* **67**, 529 (1994).
- <sup>18</sup>F. J. Himpsel, U. O. Karlsson, A. B. McLean, L. J. Terminello, F. M. F. de Groot, M. Abbate, J. C. Fuggle, J. A. Yarmoff, B. T. Thole, and G. A. Sawatzky, *Phys. Rev. B* **43**, 6899 (1991).
- <sup>19</sup>S. P. Cramer, F. M. F. DeGroot, Y. Ma, C. T. Chen, F. Sette, C. A. Kipke, D. M. Eichhorn, M. K. Chan, and W. H. Armstrong, *J. Am. Chem. Soc.* **113**, 7937 (1991).
- <sup>20</sup>H. Wang, G. Peng, L. M. Miller, E. M. Scheuring, S. J. George, M. R. Chance, and S. P. Cramer, *J. Am. Chem. Soc.* **119**, 4921 (1997).
- <sup>21</sup>S. Friedrich, O. B. Drury, T. Funk, D. Sherrell, V. K. Yachandra, S. E. Labov, and S. P. Cramer, *AIP Conf. Proc.* **705**, 985 (2004).
- <sup>22</sup>E. C. Wasinger, F. M. F. de Groot, B. Hedman, K. O. Hodgson, and E. I. Solomon, *J. Am. Chem. Soc.* **125**, 12894 (2003).
- <sup>23</sup>R. K. Hocking, E. C. Wasinger, Y.-L. Yan, F. M. F. deGroot, F. Ann Walker, K. O. Hodgson, B. Hedman, and E. I. Solomon, *J. Am. Chem. Soc.* **129**, 113 (2007).
- <sup>24</sup>F. Zheng, V. Pérez-Dieste, J. L. McChesney, Y.-Y. Luk, N. L. Abbott, and F. J. Himpsel, *Surf. Sci.* **587**, L191 (2005).
- <sup>25</sup>V. Pérez-Dieste, J. N. Crain, A. Kirakosian, J. L. McChesney, E. Arenholz, A. T. Young, J. D. Denlinger, D. L. Ederer, T. A. Callcott, S. A. Lopez-Rivera, and F. J. Himpsel, *Phys. Rev. B* **70**, 085205 (2004).
- <sup>26</sup>B. T. Thole, G. V. D. Laan, and P. H. Butler, *Chem. Phys. Lett.* **149**, 295 (1988).
- <sup>27</sup>P. L. Cook, P. S. Johnson, X. Liu, A.-L. Chin, and F. J. Himpsel, "Radiation effects on biomimetic dye molecules for solar cells," *J. Chem. Phys.* (in press).
- <sup>28</sup>R. Brydson, H. Sauer, W. Engel, J. M. Thomass, E. Zeitler, N. Kosugi, and H. Kuroda, *J. Phys.: Condens. Matter* **1**, 797 (1989).
- <sup>29</sup>C. T. Chen, N. V. Smith, and F. Sette, *Phys. Rev. B* **43**, 6785 (1991).
- <sup>30</sup>G. Dufour, C. Poncey, F. Rochet, H. Roulet, M. Sacchi, M. De Santis, and M. De Crescenzi, *Surf. Sci.* **319**, 251 (1994).
- <sup>31</sup>R. Naito, S. Toyoshima, T. Ohashi, T. Sakurai, and K. Akimoto, *Jpn. J. Appl. Phys.* **47**, 1416 (2008).
- <sup>32</sup>E. E. Koch, Y. Jugnet, and F. J. Himpsel, *Chem. Phys. Lett.* **116**, 7 (1985).
- <sup>33</sup>J. E. Downes, C. McGuinness, P.-A. Glans, T. Learnmonth, D. Fu, P. Sheridan, and K. E. Smith, *Chem. Phys. Lett.* **390**, 203 (2004).
- <sup>34</sup>Y. Zhang, S. Wang, T. Learnmonth, L. Plucinski, A.Y. Matsuura, S. Bernardis, C. O'Donnell, J. E. Downes, and K. E. Smith, *Chem. Phys. Lett.* **413**, 95 (2005).
- <sup>35</sup>Y. Zhang, T. Learnmonth, S. Wang, A. Y. Matsuura, J. Downes, L. Plucinski, S. Bernardis, C. O'Donnell, and K. E. Smith, *J. Mater. Chem.* **17**, 1276 (2007).
- <sup>36</sup>J. Åhlund, K. Nilson, J. Schiessling, L. Kjeldgaard, S. Berner, N. Mårtensson, C. Puglia, B. Brena, M. Nyberg, and Y. Luo, *J. Chem. Phys.* **125**, 034709 (2006).
- <sup>37</sup>P. Palmgren, K. Nilson, S. Yu, F. Hennies, T. Angot, C. I. Nlebedim, J.-M. Layet, G. Le Lay, and M. Göthelid, *J. Phys. Chem. C* **112**, 5972 (2008).
- <sup>38</sup>S. Krasnikov, A. B. Preobrajenski, N. N. Sergeeva, M. M. Brzhezinskaya, M. A. Nesterov, A. A. Cafolla, M. O. Senge, and A. S. Vinogradov, *Chem. Phys.* **332**, 318 (2007).
- <sup>39</sup>H. Höchst, A. Goldmann, S. Hüfner, and H. Malter, *Phys. Status Solidi B* **76**, 559 (1976).
- <sup>40</sup>G. V. Ouedraogo, D. Benlian, and L. Porte, *J. Chem. Phys.* **73**, 642 (1980).
- <sup>41</sup>A. Ruocco, F. Evangelista, R. Gotter, A. Attili, and G. Stefani, *J. Phys. Chem. C* **112**, 2016 (2008).
- <sup>42</sup>F. L. Battye, A. Goldmann, and L. Kasper, *Phys. Status Solidi B* **80**, 425 (1977) (b).
- <sup>43</sup>J. Berkowitz, *J. Chem. Phys.* **70**, 2819 (1979).
- <sup>44</sup>H. Yoshida, K. Tsutsumi, and N. Sato, *J. Electron Spectrosc. Relat. Phenom.* **121**, 83 (2001).
- <sup>45</sup>D. E. Barlow, L. Scudiero, and K. W. Hipps, *Langmuir* **20**, 4413 (2004).
- <sup>46</sup>C. Tao, J. Sun, X. Zhang, R. Yamachika, D. Wegner, Y. Bahri, G. Samsonidze, S. Louie, T. Tilly, R. Segalman, and M. Crommie, American Physical Society March Meeting, 2009 (unpublished).
- <sup>47</sup>X. Wang, C. R. Randall, G. Peng, and S. P. Cramer, *Chem. Phys. Lett.* **243**, 469 (1995).
- <sup>48</sup>S. Narioka, H. Ishii, Y. Ouchi, T. Yokoyama, T. Ohta, and K. Seki, *J. Phys. Chem.* **99**, 1332 (1995).
- <sup>49</sup>G. Polzonetti, V. Carravetta, G. Iucci, A. Ferri, G. Paolucci, A. Goldoni, P. Parent, C. Laffon, and M. V. Russo, *Chem. Phys.* **296**, 87 (2004).
- <sup>50</sup>H. Wende, M. Bernien, J. Luo, C. Sorg, N. Ponpandian, J. Kurde, J. Miguel, M. Piantek, X. Xu, Ph. Eckhold, W. Kuch, K. Baberschke, P. M. Panchmatia, B. Sanyal, P. M. Oppeneer, and O. Eriksson, *Nature Mater.* **6**, 516 (2007).
- <sup>51</sup>H. I. Liu, M. Sono, S. Kadkhodayan, L. Hager, B. Hedman, K. O. Hodgson, and J. H. Dawson, *J. Biol. Chem.* **270**, 10544 (1995).
- <sup>52</sup>M.-C. Cheng, A. M. Rich, R. S. Armstrong, P. J. Ellis, and P. A. Lay, *Inorg. Chem.* **38**, 5703 (1999).
- <sup>53</sup>F. Boffi, A. Bonincontro, S. Cinelli, A. Congui Castellano, A. De Francesco, S. Della Longa, M. Girasole, and G. Onori, *Biophys. J.* **80**, 1473 (2001).
- <sup>54</sup>I. Diaz-Moreno, A. Diaz-Quintana, G. Subias, T. Mairs, M. A. De la Rosa, and S. Diaz-Moreno, *FEBS Lett.* **580**, 3023 (2006).
- <sup>55</sup>L. Giachini, F. Francia, L. Cordone, F. Boscherini, and G. Venturoli, *Biophys. J.* **92**, 1350 (2007).
- <sup>56</sup>P. M. Kozłowski, T. G. Spiro, A. Berces, and M. Z. Zgierski, *J. Phys. Chem. B* **102**, 2603 (1998).
- <sup>57</sup>G. Peng, H. J. J. van Elp, L. Que, Jr., W. H. Armstrong, and S. P. Cramer, *J. Am. Chem. Soc.* **117**, 2515 (1995).
- <sup>58</sup>A. Curioni, W. Andreoni, R. Treusch, F. J. Himpsel, E. Haskal, P. Seidler, C. Heske, S. Kakar, T. van Buuren, and L. J. Terminello, *Appl. Phys. Lett.* **72**, 1575 (1998).
- <sup>59</sup>A. Weber-Bargioni, W. Auwärter, F. Klappenberger, J. Reichert, S. Lefrançois, T. Strunskus, C. Wöll, A. Schiffrin, Y. Pennec, and J. V. Barth, *ChemPhysChem* **9**, 89 (2008).
- <sup>60</sup>A. Ghosh, T. Vangberg, E. Gonzalez, and P. Taylor, *J. Porphyr. Phthalocyanines* **5**, 345 (2001).
- <sup>61</sup>S. Carniato, Y. Luo, and H. A. Gren, *Phys. Rev. B* **63**, 085105 (2001).
- <sup>62</sup>J. K. Park, H. R. Lee, J. Chen, H. Shinokubo, A. Osuka, and D. Kim, *J. Phys. Chem. C* **112**, 16691 (2008).
- <sup>63</sup>C.-Y. Lin, C.-F. Lo, L. Luo, H.-P. Lu, C.-S. Hung, and E. W.-G. Diau,

[J. Phys. Chem. C](#) **113**, 755 (2009).

<sup>64</sup>T. Okajima, Y. Yamamoto, Y. Ouchi, and K. Seki, [J. Electron Spectrosc.](#)

[Relat. Phenom.](#) **114–116**, 849 (2001).

<sup>65</sup>M. L. Gordon, G. Cooper, C. Morin, T. Araki, C. C. Turci, K. Ka-

znatcheev, and A. P. Hitchcock, [J. Phys. Chem. A](#) **107**, 6144 (2003).

<sup>66</sup>X. Liu, C.-H. Jang, F. Zheng, A. Jürgensen, J. D. Denlinger, K. A. Dickson, R. T. Raines, N. L. Abbott, and F. J. Himpsel, [Langmuir](#) **22**, 7719 (2006).